

Separation of ultrafast spin currents and spin-flip scattering in Co/Cu(001) driven by femtosecond laser excitation employing the complex magneto-optical Kerr effect

J. Wieczorek,¹ A. Eschenlohr,¹ B. Weidtmann,¹ M. Rösner,² N. Bergard,¹ A. Tarasevitch,¹ T. O. Wehling,² and U. Bovensiepen^{1,*}

¹*Faculty of Physics and Center for Nanointegration (CENIDE), University of Duisburg-Essen, Lotharstrasse 1, 47057 Duisburg, Germany*

²*Institute for Theoretical Physics, Bremen Center for Computational Materials Science, University of Bremen, Otto-Hahn-Allee 1, 28359 Bremen, Germany*

(Received 22 December 2014; revised manuscript received 15 September 2015; published 9 November 2015)

Ultrafast magnetization dynamics in metallic heterostructures consists of a combination of local demagnetization in the ferromagnetic constituent and spin-dependent transport contributions within and in between the constituents. Separation of these local and nonlocal contributions is essential to obtain microscopic understanding and for potential applications of the underlying microscopic processes. By comparing the ultrafast changes of the polarization rotation and ellipticity in the magneto-optical Kerr effect we observe a time-dependent magnetization profile $M(z,t)$ in Co/Cu(001) films by exploiting the effective depth sensitivity of the method. By analyzing the spatiotemporal correlation of these profiles we find that on time scales before hot electron thermalization (<100 fs) the transient magnetization of Co films is governed by spin-dependent transport effects, while after hot electron thermalization (>200 fs) local spin-flip processes dominate.

DOI: [10.1103/PhysRevB.92.174410](https://doi.org/10.1103/PhysRevB.92.174410)

PACS number(s): 75.78.Jp, 72.25.Ba, 78.20.Ls

I. INTRODUCTION

Electronic excitations in ferromagnets are essentially spin polarized. In the transition-metal ferromagnets Fe, Co, and Ni excitations of 0.1–1 eV relax on femto- to picosecond time scales [1,2] due to scattering with secondary excitations mediated by electron-phonon, electron-magnon, and electron-electron / exchange interaction. The underlying microscopic processes are essential in ultrafast magnetization dynamics [3,4].

Recently, this field has been propelled by ultrafast spin polarized [5–10] and unpolarized currents [11] generated by a gradient in excitation density [12]. These effects offer exploiting nonlocal magnetization dynamics. Already now femtosecond (fs) laser-excited spin currents in layer stacks were reported to induce spin transfer torque [13]. Furthermore, laser-induced spin currents in a magnetic tunnel junction were controlled by a bias voltage [14]. Moreover, spin currents are reported to drive an ultrafast change between ferri- and ferromagnetic order [10].

Such demonstrations suggest an extension of spintronics, including spin filter and magnetoresistance effects, into the nonequilibrium regime. In turn, fs time-resolved experiments allow conclusions on spin transport [5,7–9,11], to shed light on the underlying microscopic mechanisms. However, so far experimental means to distinguish ultrafast spin currents, which propagate into conducting contacts/substrates from ferromagnetic layers, and competing depolarizing spin-flip scattering, which reduces the magnetization M in these spin current sources, are missing.

Here we show how to fill this gap by establishing that laser-excited spin currents result in a specific transient magnetization profile $M(z,t)$ in the direction z along the film normal, before spin flips impact the dynamics. We employ ferromagnetic Co/Cu(001) films as a model system for a spin current source

contacted by a spin sink. Key is the combined analysis of the film thickness dependence with the time-dependent difference in polarization rotation θ and ellipticity ϵ of the magneto-optical Kerr effect (MOKE), which provides a depth sensitivity and access to $M(z,t)$. We separate spin currents generated by nonthermalized carriers up to ~ 100 fs and local demagnetization due to spin-flip scattering of thermalized carriers dominant after ~ 200 fs.

A contested issue in ultrafast MOKE is whether the observations reflect $M(t)$, or transient changes of the optical constants. Koopmans *et al.* [15], finding that θ and ϵ of the complex Kerr angle $\Phi = \theta + i\epsilon$ showed a different behavior for $t \leq 100$ fs, assigned the difference to state-filling effects. Later, Guidoni *et al.* [16] reported that the magneto-optical response is dominated by the magnetization dynamics after electron thermalization. However, the origin of the transient difference between θ and ϵ before thermalization has so far been unclear [16]. We derive that the transient difference of θ and ϵ on femtosecond time scales is a result of a spatial profile in the magnetization.

Also, the relative importance of (i) spin-flip scattering of thermalized electrons, described by the microscopic three-temperature model (M3TM) [17], and (ii) superdiffusive spin transport [6,18,19] of hot, nonequilibrium electrons, in ultrafast magnetization dynamics, is under discussion. Experiments on layered structures have demonstrated the importance of spin transport [5,7–9,11], while demagnetization of metallic films on insulators was ascribed to spin flips [20], leading to an emerging consensus that both processes play a role [21]. Here, we investigate both spin-flip processes confined to the ferromagnetic film, as well as propagating spin currents that are accepted by the metallic substrate, in a model system.

II. ANALYSIS OF TRANSIENT MAGNETIZATION GRADIENTS

Femtosecond laser excitation of heterostructures such as Co/Cu(001) epitaxial films, which present a large gradient

*uwe.bovensiepen@uni-due.de

in spin polarization from the film to the substrate already in equilibrium, leads to spatial redistribution of charge carriers [12,22] and spin polarization by transport effects in particular across the interface [6,7,21]. Locally within the ferromagnetic film the magnetization changes also by spin-flip scattering. In order to quantify the spin-dependent transport processes compared to local demagnetization we first estimate these two contributions by analytical calculations in one dimension along the interface normal direction. Lateral magnetization gradients within the film plane are also present due to the lateral gradient in excitation density following the laser focus with a full width at half maximum, in the present case, of about $16 \mu\text{m}$. However, since these lateral gradients are three orders of magnitude smaller than the one along the normal direction, we neglect them here and consider only the normal component, which is essential for the subpicosecond dynamics.

A. Estimation of spin diffusion and local demagnetization contributions

In Fig. 1(a) we contrast the relative local magnetization $m(z,t) = M(z,t)/M_0$ for (i) spin-flip scattering of thermalized electrons and (ii) spin transport, calculated with an extended M3TM and a spin diffusion equation, respectively. M_0 is the homogeneous equilibrium magnetization.

To estimate the spin-flip contribution we start with calculating the time- and spatially dependent electronic and lattice temperatures, $T_e(z,t)$ and $T_l(z,t)$, respectively, for different Co film thicknesses d on Cu(001) employing a two-temperature model (2TM) [23]. We include electronic heat diffusion, which is driven by the spatial gradient in the electronic temperature [23], and account for the Co film with thickness d . We further include the Cu substrate in the calculation. We take the optical penetration depth δ_{skin} of the pump pulse at 800 nm central wavelength into account and include thereby the position-dependent optical absorption in the calculation. The initial excitation profile in cobalt and copper was calculated by

$$S(z,t) = \frac{F_{\text{abs},i} e^{-z/\delta_{\text{skin},i}}}{\delta_{\text{skin},i} (1 - e^{-d_i/\delta_{\text{skin},i}})} G(t). \quad (1)$$

$G(t)$ is a normalized Gaussian function with a FWHM of 35 fs, and d_i is the film thickness, where i stands for cobalt and copper. For copper we used $d_{\text{Cu}} = \infty$. The penetration depth of the laser $\delta_{\text{skin,Co}} = 13 \text{ nm}$ and $\delta_{\text{skin,Cu}} = 12 \text{ nm}$ was calculated according to the optical constants $n_{\text{Co}} = 2.56 + i4.92$ and $n_{\text{Cu}} = 0.26 + i5.26$ [24]. These optical constants were also used to calculate the absorbed fluence $F_{\text{abs},i}$ employing [25], where we set the incident fluence to $F_{\text{in}} = 3 \text{ mJ/cm}^2$.

Subsequently, we used the M3TM, which considers spin-flip scattering only for a thermalized electronic system, to obtain dm_{M3TM}/dt and $m_{\text{M3TM}}(z,t)$ [17]. To take the thermalization time of the electronic system in the simulation for the spin-flip scattering into account, we multiply the expression dm_{M3TM}/dt from the M3TM [17] with a time-dependent factor $n_{\text{therm}}(t)$ [22]. It was calculated with $n_{\text{hot}}/dt = G(t) - n_{\text{hot}}/\tau_{\text{therm}}$ and $dn_{\text{therm}}/dt = n_{\text{hot}}/\tau_{\text{therm}}$, where $n_{\text{hot}}(t)$ and $n_{\text{therm}}(t)$, referring to the fractions of hot, nonequilibrium, and thermalized electrons,

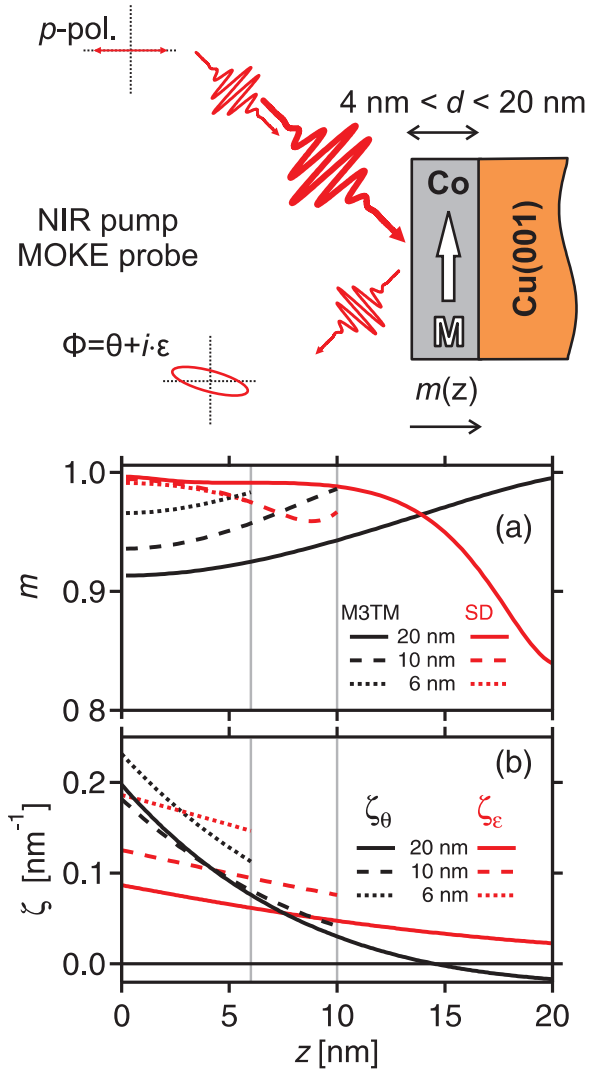


FIG. 1. (Color online) Top: Kerr rotation and ellipticity of Co/Cu(001) are measured in a pump-probe experiment. (a) Normalized magnetization profile $m(z)$ calculated with the M3TM [17] (black) for $t_0 = 170 \text{ fs}$ and spin diffusion (SD, red) for $t_0 = 20 \text{ fs}$. (b) MOKE sensitivity $\zeta(z)$ for the real part/rotation $\zeta_\theta(z)$ (black) and imaginary part/ellipticity $\zeta_\epsilon(z)$ (red). The respective curves are shown for Co thicknesses d of 6 (dotted), 10 (dashed), 20 nm (solid lines).

respectively, are factors between $0 < n < 1$, $G(t)$ is a normalized Gaussian function with a FWHM of 35 fs, and $\tau_{\text{therm}} = 150 \text{ fs}$ is the thermalization time of the electronic system, which is a typical time for a $3d$ metal [26]. The used parameters are the electron-phonon coupling constants $g_{\text{Co}} = 9.3 \times 10^7 \text{ W/m}^3 \text{ K}$, $g_{\text{Cu}} = 10^7 \text{ W/m}^3 \text{ K}$ [27], the electronic heat capacity coefficients $\gamma_{\text{Co}} = 4.4 \text{ mJ/mol K}^2$, $\gamma_{\text{Cu}} = 0.69 \text{ mJ/mol K}^2$ [28], the specific heats for $T \rightarrow \infty$ $C_{\text{Co}} = 24.81 \text{ J/mol K}$, $C_{\text{Cu}} = 24.43 \text{ J/mol K}$, the Debye temperatures $\Theta_{\text{Co}} = 386 \text{ K}$, $\Theta_{\text{Cu}} = 310 \text{ K}$ [29], the mass densities $\rho_{\text{Co}} = 8.86 \text{ g/cm}^3$, $\rho_{\text{Cu}} = 8.96 \text{ g/cm}^3$ [30], the molar masses $M_{\text{Co}} = 58.93 \text{ g/mol}$, $M_{\text{Cu}} = 63.55 \text{ g/mol}$ [31], the thermal conductivities $\kappa_{\text{Co}} = 100 \text{ W/m K}$, $\kappa_{\text{Cu}} = 400 \text{ W/m K}$ [29], the Curie temperature of Co $T_C = 1388 \text{ K}$ [32], and the M3TM scaling factor for the demagnetization rate of Co $R = 25.3 \text{ ps}^{-1}$ [17].

To simulate spin diffusion (SD) we employ a diffusion equation for excited electrons based on Fick's second law [33] for majority and minority electrons. Equation (2) contains the respective source, diffusion, and decay terms. We discard charge current contributions because contrary to dielectrics a potential charge current which is linked to the spin current is screened in metals already on time scales slower than the inverse plasma frequency. In Co these time scales were concluded to be sub-fs [34] and are thus well below our experimental time resolution. We use the diffusion coefficient $D_\sigma = v_\sigma \lambda_\sigma / 3$, σ represents majority and minority electrons, for self diffusion to simulate the transport. The respective mean free path along z is $\lambda_\sigma = v_\sigma \tau_\sigma$. Velocities v_σ and lifetimes τ_σ were averaged up to 0.5 eV above the Fermi level E_F which is reasonable to account for spin diffusion considering that the experimentally determined scattering times reported in Refs. [1,2] refer to primary excited electrons. An electron at an energy of $E - E_F = 1$ eV has, e.g., a lifetime below 10 fs. Within our time resolution, such a primary excited electron will have scattered more than once and lowered its energy accordingly. We used energy-averaged lifetimes $\tau_\uparrow = 22$ fs and $\tau_\downarrow = 20$ fs which were determined from Ref. [2]. The velocities were calculated by density functional calculations (see Appendix) which resulted in energy-averaged velocities $v_\uparrow = 0.6$ nm/fs and $v_\downarrow = 0.2$ nm/fs. Taking these values for λ_σ and v_σ we obtained the considered diffusion constants $D_\uparrow = 2.4$ m²/fs, $D_\downarrow = 0.27$ m²/fs. We finally calculate the spin diffusion by

$$\frac{\partial n_\sigma}{\partial t} = D_\sigma \frac{\partial^2 n_\sigma}{\partial z^2} + c_\sigma S_\sigma(z,t) - \frac{n_\sigma}{\tau_{el}}, \quad (2)$$

where n_σ is the density of excited electrons, and $c_\sigma S_\sigma(z,t)$ describes fs laser excited primary and subsequently generated secondary electrons with c_σ being a constant factor. To account for the spatial distribution, we convoluted two exponential decay terms according to the position-dependent absorption due to the optical penetration length δ_{skin} and the spin-dependent mean free path $\lambda_{ball,\sigma}$ of primary excited electrons [35]. The latter is determined by ballistic velocities and lifetimes which were taken at energies of the maximum excitation probability in the joint density of states; see Appendix. The values are $v_{ball,\uparrow} = 1$ nm/fs, $v_{ball,\downarrow} = 0.3$ nm/fs and $\tau_{ball,\uparrow} = 18$ fs, $\tau_{ball,\downarrow} = 6$ fs [2]. Then, $\lambda_{ball,\sigma}$ was calculated with the respective velocities and lifetimes. We included propagation in Cu with $\lambda = 70$ nm [35] by setting $n_\sigma = 0$ since bulk Cu acts as an efficient electron and spin drain. The last term $-n_\sigma/\tau_{el}$ describes electron thermalization and spin current decay by a time constant τ_{el} . As an effective decay time of the spin-polarized current we took a value of $\tau_{el} = 100$ fs [18]. The change $\partial m_{SD}/\partial t$ is defined through the balance of the magnetic moments of in- and outgoing electrons.

Comparing the magnetization profiles resulting from local spin-flip scattering and spin transport, as depicted in Fig. 1(a), $m(z,t_0)$ are strikingly and systematically different for the two scenarios because the respective gradients $\partial m(z,t_0)/\partial z$ have an opposite sign. While consideration of spin-flip scattering of thermalized electrons results in a minimum m at the surface and a maximum at the Co-Cu interface, the spin diffusion description leads to a depletion of m at the interface in combination with a weak variation near the surface, in

good agreement with a more sophisticated description by superdiffusive spin transport [18].

B. Measurement of the spatiotemporal magnetization dynamics

To analyze $m(z,t)$ experimentally, we measured the complex MOKE $\Phi = \theta + i\epsilon$ in a pump-probe experiment; see Fig. 1 (top). The magneto-optical (MO) Kerr rotation θ and the ellipticity ϵ were determined by a polarization analysis using a balance detection scheme. We employed a cavity dumped Ti:sapphire oscillator which generates p-polarized 35 fs laser pulses at $h\nu = 1.55$ eV and 40 nJ pulse energy, that are split into pump and probe pulses at a 4:1 ratio, at 2.53 MHz repetition rate. The incident pump fluence was 6 mJ/cm². Further details of the experimental setup are given in Refs. [36,37]. Epitaxial Co films of 4 nm $< d < 20$ nm, which we investigated *in situ*, were grown in ultrahigh vacuum on Cu(001) following Ref. [38]. The film's easy axis of the magnetization lies in the film plane and we measure MOKE in the longitudinal geometry.

We find different transient responses of $\theta(t)$ and $\epsilon(t)$, shown in Fig. 2. Our following conclusions are based on the fact that Kerr rotation θ and ellipticity ϵ exhibit different depth sensitivities which we use to identify specific magnetization profiles $m(z,t)$ caused by spin-flip scattering of thermalized electrons or spin-polarized currents; see Fig. 1(a). In Fig. 1(b) we plot $\zeta = \zeta_\theta + i\zeta_\epsilon$, which we term MOKE sensitivity for the complex Kerr angle $\Phi = \theta + i\epsilon$, as a function of the position z within a 6, 10, and 20 nm thick film. The sensitivity ζ indicates how changes $\Delta m(z,t) = m(z,t) - 1$ contribute at a depth z in first order to the total change. The measured transient changes in Φ are calculated by integration over the Co film thickness

$$\Delta\theta(t)/\theta_0 + i\Delta\epsilon(t)/\epsilon_0 = \int_0^d \zeta(z)\Delta m(z,t)dz. \quad (3)$$

Following Traeger *et al.* [39], $\zeta(z)$ was calculated by setting $m = 0$ with the exception of a part $z, z + dz$ where $m = 1$, and determining the complex Kerr angle of this part $\Phi_{dz} = \theta_{dz} + i\epsilon_{dz}$ for this system. To take pump-induced changes into account we normalized Φ_{dz} to the equilibrium values and obtain

$$\zeta(z)dz = \frac{\theta_{dz}}{\theta_0} + i\frac{\epsilon_{dz}}{\epsilon_0}. \quad (4)$$

We used the matrix formalism by Zak *et al.* [40] with $dz = 0.2$ nm and refractive indices n_{Cu} and n_{Co} . The static MO constant q_{Co} which enters the determination of ζ was determined experimentally to $q_{Co} = 0.017 - i0.020$ by fitting the thickness-dependent MO contrast and the ratio ϵ/θ for $d = 4-20$ nm (not shown).

Note that ζ_θ is larger near the surface than near the Co-Cu interface and ζ_ϵ exhibits a weaker z dependence; see Fig. 1(b). Applying Eq. (3) reveals that (i) θ probes effectively the near-surface part. For thicker layers such as 20 nm the sign of the rotation sensitivity eliminates some signal contribution from the bulk part of the film which also leads to an effective probing of the near-surface region. (ii) The second magneto-optical observable ϵ rather averages over the film and includes a sensitivity at the Co/Cu interface. This depth dependence of ζ provides us with a probe for $m(z,t)$.

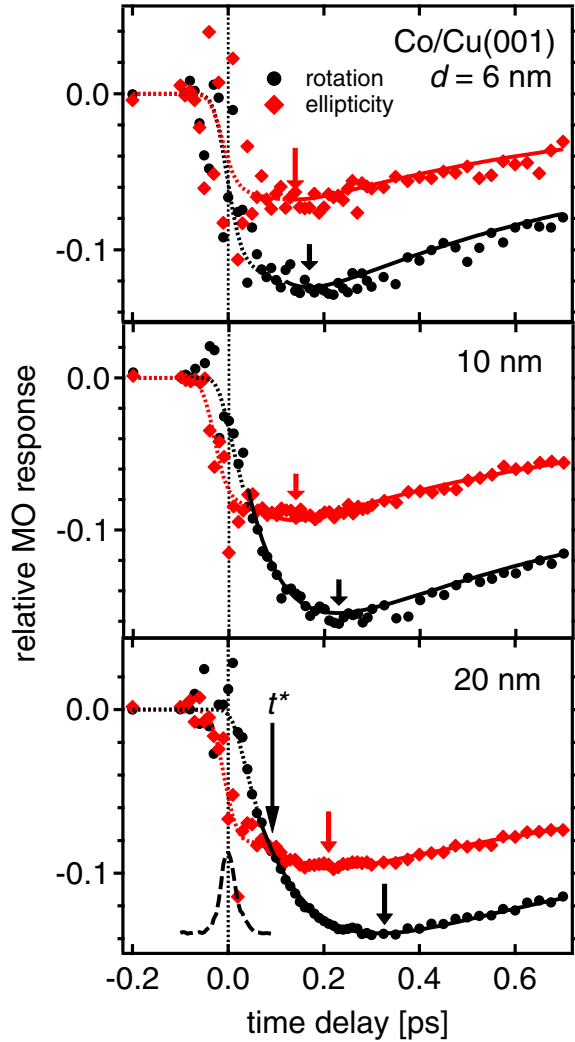


FIG. 2. (Color online) Time-dependent relative MO responses of Kerr rotation $\Delta\theta(t)/\theta_0$ (dots) and ellipticity $\Delta\epsilon(t)/\epsilon_0$ (diamonds) of Co/Cu(001) for $d = 6, 10, 20$ nm. Solid lines represent analytical fit functions, while dotted lines guide the eye. For determination of $t = 0$ we measured the autocorrelation function with second harmonic generation from the surface (dashed line, bottom panel). Arrows indicate the delay of minimum MO response; t^* indicates when $\Delta\theta(t)/\theta_0 = \Delta\epsilon(t)/\epsilon_0$.

Now we consider our experimental results in detail. Figure 2 depicts the time-dependent relative MO responses $\Delta\theta(t)/\theta_0$ and $\Delta\epsilon(t)/\epsilon_0$ for Co/Cu(001) for $d = 6, 10, 20$ nm. The curves show a reduction of the signal which begins within the laser pulse and a subsequent recovery starting between 100 and 300 fs, depending on the film thickness. Most importantly, we find for all d differences for $\theta(t)$ and $\epsilon(t)$. For $d \geq 10$ nm we observe a faster reduction of ϵ than for θ and a crossing at delay t^* of both curves within 200 fs. After this crossing the changes are inverted relative to each other and $\Delta\theta(t)/\theta_0$ remains stronger than $\Delta\epsilon(t)/\epsilon_0$ up to 25 ps. This remaining difference will be addressed further below. For $d < 10$ nm the initially stronger reduction of ϵ compared to θ is not observed, likely due to a limited pulse duration and a remainder of the coherent artifact [41], in combination

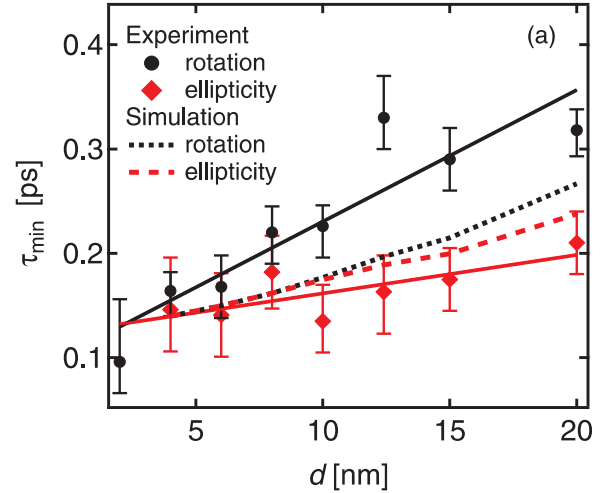


FIG. 3. (Color online) (a) Time delay τ_{\min} of minimal response in $\Delta\theta(t)/\theta_0$ (black dots) and $\Delta\epsilon(t)/\epsilon_0$ (red diamonds) vs d . Solid lines are linear fits, dashed lines depict simulations.

with a weaker dm/dz . Changes for such d are larger in θ than in ϵ .

From the observed $\theta(t)$ and $\epsilon(t)$ we conclude on $m(z, t)$ and relate this to a spin-polarized current or spin-flip scattering; see Fig. 1(a). Here, the different depth sensitivity of θ and ϵ , see Fig. 1(b), is essential. Remember, ϵ exhibits a stronger sensitivity at the Co/Cu interface than θ . The stronger reduction of the ellipticity compared to the rotation starting within the pulse duration, see Fig. 2, thus implies that the film is demagnetized more near the inner interface than near the surface. The respective magnetization profile agrees qualitatively with the one obtained for SD; see Fig. 1(a). After some tens of femtoseconds, depending on d , $m(z, t)$ is concluded to be redistributed towards a profile expected from the M3TM [17], as can be seen in the larger variation of θ compared to ϵ in Fig. 2 at $t > t^*$, taking into account that θ has a higher sensitivity at the surface than ϵ ; see Fig. 1(b). These transient changes of the magnetization profile suggest that when the electronic system has not yet thermalized, a spin-polarized current dominates $m(z, t)$. With electron thermalization, spin-flip events take over. This is consistent with both the superdiffusive transport model [18] and the M3TM [17]. The superdiffusive transport model predicts spin transport for a nonthermalized electron system, which recedes with thermalization [42], while the M3TM considers only thermalized electrons, which contribute to spin-flip scattering [17].

Our conclusions are corroborated by finding that the time delay τ_{\min} of the minimum MO response exhibits a systematic thickness dependence, as depicted in Fig. 2. To determine this delay of the minimum response we performed a fitting analysis and determined τ_{\min} using $f(t) = A_M[1 - \exp(-t/\tau_M)] + A_{R1}[1 - \exp(-t/\tau_{R1})] + A_{R2}[1 - \exp(-t/\tau_{R2})]$; A and τ are the amplitudes and time constants, respectively; $M, R1, R2$ refer to demagnetization and recovery [43]. For ϵ and θ the minimum positions shift to later times with increasing d ; see Fig. 3. Particularly interesting is the different thickness dependence of ϵ and θ . By fitting the minimum's position as a function of d with a line, we find with slopes of

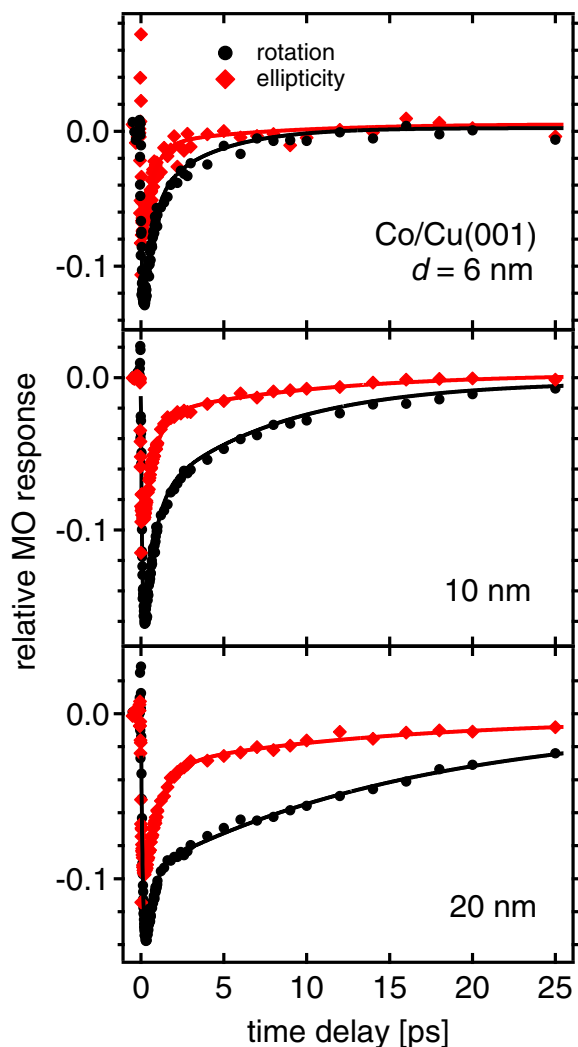


FIG. 4. (Color online) Time-dependent relative magneto-optical responses of Kerr rotation $\Delta\theta(t)/\theta_0$ (dots) and ellipticity $\Delta\epsilon(t)/\epsilon_0$ (diamonds) of Co/Cu(001) for $d = 6, 10, 20$ nm for pump-probe delays of up to 25 ps. Solid lines represent analytical fits described in the text.

$b_\theta = 13$ fs/nm and $b_\epsilon = 4$ fs/nm a pronounced, three time difference.

Figure 4 shows time-dependent MOKE data for longer time delays up to 25 ps for selected film thicknesses. The difference between the MOKE ellipticity and rotation remains clearly longer than 5 ps and the time delay of merging of the two observables shifts to later delays with increasing film thickness. Considering typical electronic relaxation or electron-lattice equilibration times of a few ps suggests that this difference cannot be fully explained by the competition of spin diffusion and local demagnetization. We will come back to this aspect in the discussion section.

C. Model description of the spatiotemporal magnetization dynamics

We simulated the thickness-dependent $m(z,t)$ with the extended M3TM [17] and the spin-polarized diffusion equation,

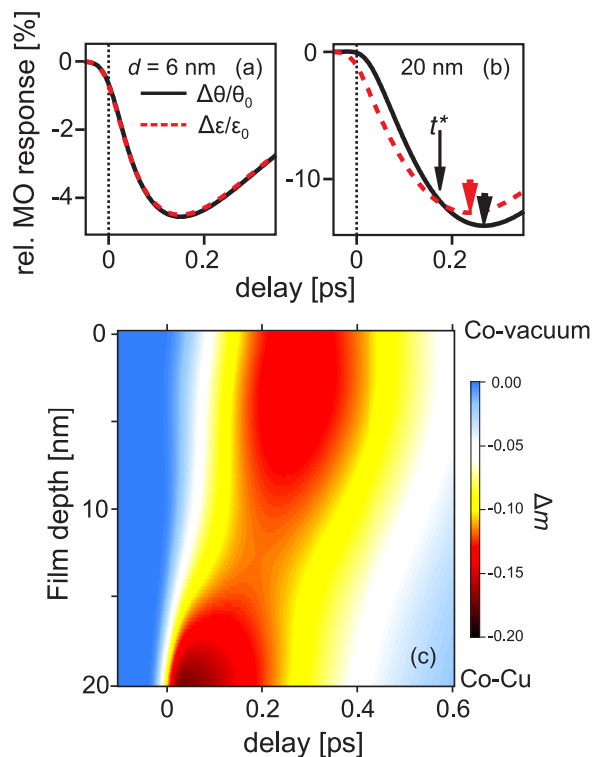


FIG. 5. (Color online) (a), (b) Simulated magneto-optical response $\Delta\theta(t)/\theta_0$ (solid) and $\Delta\epsilon(t)/\epsilon_0$ (dashed) for $d = 6, 20$ nm. (c) Simulated spatiotemporal variation of the relative magnetization change Δm for a 20 nm thick Co film on Cu(001) in a false-color representation as a function of time delay and position within the film.

as introduced above, by adding both contributions:

$$\frac{dm(z,t)}{dt} = \frac{\partial m_{\text{M3TM}}(z,t)}{\partial t} + \frac{\partial m_{\text{SD}}(z,t)}{\partial t}. \quad (5)$$

We calculated the corresponding MO response with Eq. (3) using the parameters given above in Sec. II.A, and determined the delays of minimum MO response as a function of film thickness d , which are included in Fig. 3 as dashed lines. The overall shift of τ_{min} to later times with increasing d is explained by the lower heat conductivity of Co compared to Cu [29]. Essential for the discussion of the competing spin-dependent processes is the thickness-dependent difference between τ_{min} for θ and ϵ , which is qualitatively reproduced by our simulation. The Co-Cu interface region, which is preferentially probed by ϵ , reaches the minimum magnetization earlier and also starts to recover earlier. Consequently, this confirms our above explanation of the initial dynamics by spin transport near the Co/Cu interface and the later dynamics by spin-flip scattering at the surface. We qualitatively reproduce the transient behavior of our MO observables already with such a relatively simple model up to delays of 400 fs when the electronic system is in nonequilibrium with respect to the lattice. In Figs. 5(a) and 5(b) we show two simulations of $\Delta\theta$ and $\Delta\epsilon$ for $d = 6, 20$ nm. For 20 nm we obtain an initially faster (< 100 fs) reduction of ϵ compared to θ , and later at 200 fs the crossing of both curves. For 6 nm our simulation does not exhibit any difference for the two magneto-optical observables

which is in agreement with the experimental result as far as for these small thicknesses the minima in $\Delta\epsilon(t)/\epsilon_0$ and $\Delta\theta(t)/\theta_0$ are not discernible within the error bars. We will come back to this point in the discussion below.

Having explained the origin of the different transient behavior of the two MO observables by the two separate, elementary spin-dependent processes of spin transport from the Co film into the substrate and local spin-flip scattering within the Co film, we simulated the spatiotemporal dynamics of the magnetization change Δm as a function of position within the Co film and time delay. The result is shown in Fig. 5(c) and highlights the separate locations of the spin-flip and the spin transport processes in the near-surface region at delays just above 200 fs and near the Co-Cu interface earlier than 100 fs. Moreover, a minimum in Δm can be observed in the region near the center of the sample at around 12 nm film depth. This region is not demagnetized strongly by either of the two spin-dependent processes.

Note that we used a reduced fluence in the calculation compared to the experiment in order to adjust the calculated magnitude of demagnetization to the experimentally observed one. The relative difference between the fluence in the calculation and in the experiment is two times which is attributed to deviations of the optical constants in the epitaxial film-substrate system, limitations in the determination of the laser focus on the sample surface in the vacuum chamber, and the employed simplifications in the model.

III. DISCUSSION

The calculated behavior with spin-flip and spin current contributions agrees with the experimental observation; cf. Figs. 2, 3. For $t > t^*$, the pump-induced variation for θ is stronger than for ϵ , also in agreement with Fig. 2, and the dynamics are dominated by spin-flip scattering. This behavior is only obtained if the SD contribution is included; the M3TM alone is not sufficient. We conclude furthermore that the contributions from both mechanisms are comparable and therefore both have to be considered. However, as we demonstrate here, they can be separated in the time domain. For $d = 6$ nm we lose the sensitivity to the competing processes in the simulation, probably due to a more homogeneously demagnetized film. After all, Fig. 1(a) indicates a loss of m due to SD at the inner interface as well as spin-flip scattering at the surface both on a length scale comparable to 6 nm. In this thin-film limit the magnetization gradients resulting from spin-flip scattering and spin transport in the Co film have essentially receded. They become more similar to each other because the film thickness approaches the spin-dependent mean free path, as spins can now be transported into Cu also from regions closer to the Co surface.

The deviation of the simulation and the experimental data in Fig. 3 is potentially a result of uncertainties in the optical constants. In addition, spin-dependent back diffusion of electrons from Cu into Co [11,18], which is not included in the simulation, can enhance the demagnetization near the Co/Cu interface found in our SD simulations further. Spin-dependent scattering at defects could also contribute to the spin dynamics and would be determined by the defect density at the interface. Here, we investigate an epitaxial film

on a single crystal substrate which is the best way to avoid such defects. As the results of our simulation only show a qualitative agreement with our experimental results, see Fig. 3, such approximations might be one of the reasons for this. For a quantitative description energy and spin-dependent transmission coefficients at the interface need to be considered, as well as many-body renormalizations. This is, however, beyond the scope of this article. Likely, these aspects need to be taken into account for the deviation of the fluence used in the simulation and in the experiment.

A pump-induced variation of the optical constants due to the hot electron distribution could influence our results, but we are convinced that $m(z,t)$ dominates the dynamics. We argue as follows. (i) For films $d \geq 10$ nm the difference between θ and ϵ up to $t = 200$ fs is comparable to later times, but with opposite sign (Fig. 2). To explain this by a time-dependent change of optical constants, a change in sign at a remaining absolute value would be required. This is rather unlikely since such effects would decay monotonically with the hot electron distribution within ~ 1 ps [16,26]. (ii) With decreasing d the difference between θ and ϵ at $t < t^*$ shrinks faster than for $t > t^*$ (Fig. 2), while the hot electron distribution remains for all d . In contrast, spin-polarized transport is strongly affected by the sample thickness [7,11,18]. (iii) The difference between θ and ϵ remains up to 25 ps, see Fig. 4, which is too long for state filling effects due to a hot electron distribution, considered previously [15]. A magnetization profile $m(z,t)$, which is detected through the different ζ for θ and ϵ , can, however, remain for such a long time due to a spatial gradient in the lattice temperature. In fact, the gradient in the magnetization might persist even longer than it takes the lattice temperature to homogenize, as at longer time scales, when the excitation of the electronic system has already relaxed, changes in the magnetization due to changes in the lattice temperature are mediated by spin-lattice coupling, which is not included in the M3TM and has characteristic time scales of several ps to tens of ps.

IV. CONCLUSION AND OUTLOOK

We showed that the different depth sensitivity of the magneto-optical Kerr rotation and ellipticity can be used to identify spatial magnetization profiles on ultrafast time scales resulting from spin-polarized transport or spin-flip scattering. We found that the laser-excited spin dynamics in Co/Cu(001) films are dominated by spin transport effects on times up to ~ 100 fs when the electronic system has not yet thermalized, and by spin-flip scattering of thermalized electrons subsequently.

Since the sensitivity function, which governs the depth sensitivity, is straightforward to calculate, the demonstrated method is readily applicable to further material systems. Here, analysis of metallic ferromagnets on an insulating substrate might provide a film-substrate combination complementary to the metal-metal case discussed here. We note that for the here presented methodology it will be essential to determine the complex sensitivity function independently of other heterosystems by a full, thickness-dependent analysis, because it is set by the film-substrate combination rather than by the film alone. Moreover, an improved experimental interface sensitivity, which can be obtained by using nonlinear

optical techniques, promises direct access to the spin transfer dynamics across interfaces and might be rewarding in order to obtain deeper insight towards a full reconstruction of $m(z,t)$ and a more quantitative understanding.

ACKNOWLEDGMENTS

We are grateful for fruitful discussions with and experimental support by A. Melnikov. This work was funded by the DFG through SFB 616, the BMBF through 05K10PG2 FEMTOSPEX, and the Mercator Research Center Ruhr through Grant No. PR-2011-0003. The numerical computations were carried out on the North-German Supercomputing Alliance (HLRN) cluster.

APPENDIX

The group velocities as well as the densities of excited carriers in bulk Co were calculated within the spin-polarized generalized gradient approximation (GGA) [44] to density functional theory as implemented in the Vienna *Ab initio* Simulation Package (VASP) [45] with the projector augmented waves basis sets [46,47]. The calculations were performed with a hcp unit cell of Co (lattice constants $a \approx 2.51 \text{ \AA}$ and $c \approx 4.07 \text{ \AA}$ [48]) using $40 \times 40 \times 40 k$ meshes for the Brillouin zone integration and a plane-wave cutoff of 335 eV.

The excitation probability for an electron-hole pair formed by states $|c,k,\sigma\rangle$ (electron) and $|v,k,\sigma\rangle$ (hole) at crystal momentum k and with spin σ is calculated based on Fermi's golden rule according to

$$P(k,\sigma,c,v) \propto |M_{c,v,\sigma}^k|_{xx}^2 \delta(E_{c,k,\sigma} - E_{v,k,\sigma} - E_{\text{ex}}),$$

where $|M_{c,v,\sigma}^k|_{xx}$ are the optical transition matrix elements for electric fields polarized in the x direction, $E_{v/c,k}$ conduction

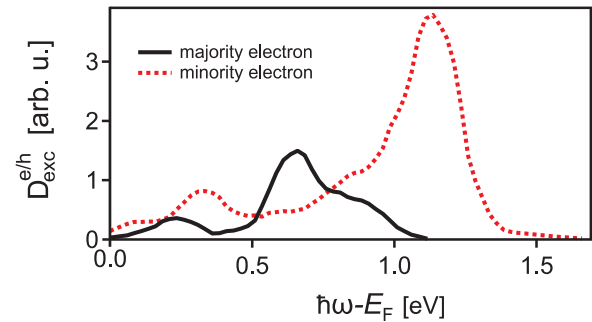


FIG. 6. (Color online) Calculated density of carriers excited in Co vs their energy with respect to the Fermi level.

and valence band energies, and $E_{\text{ex}} = 1.55 \text{ eV}$ is the laser excitation energy. We employed 0.01 eV Gaussian broadening for the evaluation of the excitation probabilities.

The energy-resolved density of excited carriers D is determined by

$$D_{\text{exc}}^{e/h}(\omega) = \frac{1}{N_k} \sum_{c,v,k} |M_k|_{xx}^2 \delta(E_{\sigma}^{c,k} - E_{\sigma}^{v,k} - E_{\text{ex}}) \times \delta(E_{\sigma}^{v/c,k} - \omega),$$

where N_k is the number of k points. Here, v and c are band indices referring to states below and above the Fermi level, respectively. The results are depicted in Fig. 6. Using the above equation we estimate the energy of primary excited electrons, which yields 0.7 eV and 1.1 eV for the majority and minority electrons, respectively. The components of the group velocities perpendicular to the surface, which enter our above simulation, are calculated according to $v_{\sigma}(E_{\sigma}) = \hbar^{-1} \partial / \partial E_{\sigma} \partial k_z$.

-
- [1] M. Aeschlimann, M. Bauer, S. Pawlik, W. Weber, R. Burgermeister, D. Oberli, and H. C. Siegmann, *Phys. Rev. Lett.* **79**, 5158 (1997).
- [2] A. Goris, K. M. Döbrich, I. Panzer, A. B. Schmidt, M. Donath, and M. Weinelt, *Phys. Rev. Lett.* **107**, 026601 (2011).
- [3] E. Beaurepaire, J.-C. Merle, A. Daunois, and J.-Y. Bigot, *Phys. Rev. Lett.* **76**, 4250 (1996).
- [4] A. Kirilyuk, A. V. Kimel, and Th. Rasing, *Rev. Mod. Phys.* **82**, 2731 (2010).
- [5] G. Malinowski, F. Dalla Longa, J. H. H. Rietjens, P. V. Paluskar, R. Huijink, H. J. M. Swagten, and B. Koopmans, *Nat. Phys.* **4**, 855 (2008).
- [6] M. Battiato, K. Carva, and P. M. Oppeneer, *Phys. Rev. Lett.* **105**, 027203 (2010).
- [7] A. Melnikov, I. Razzdolski, T. O. Wehling, E. Th. Papioannou, V. Roddatis, P. Fumagalli, O. Aktsipetrov, A. I. Lichtenstein, and U. Bovensiepen, *Phys. Rev. Lett.* **107**, 076601 (2011).
- [8] D. Rudolf *et al.*, *Nat. Commun.* **3**, 1037 (2011).
- [9] T. Kampfrath *et al.*, *Nat. Nanotechnol.* **8**, 256 (2013).
- [10] C. E. Graves *et al.*, *Nat. Mater.* **12**, 293 (2013).
- [11] A. Eschenlohr, M. Battiato, P. Maldonado, N. Pontius, T. Kachel, K. Hollmack, R. Mitzner, A. Föhlisch, P. M. Oppeneer, and C. Stamm, *Nat. Mater.* **12**, 332 (2013).
- [12] S. D. Brorson, J. G. Fujimoto, and E. P. Ippen, *Phys. Rev. Lett.* **59**, 1962 (1987).
- [13] A. J. Schellekens, K. C. Kuiper, R. R. J. C. de Wit, and B. Koopmans, *Nat. Commun.* **5**, 4333 (2014).
- [14] M. Savoini *et al.*, *Phys. Rev. B* **89**, 140402(R) (2014).
- [15] B. Koopmans, M. van Kampen, J. T. Kohlhepp, and W. J. M. de Jonge, *Phys. Rev. Lett.* **85**, 844 (2000).
- [16] L. Guidoni, E. Beaurepaire, and J.-Y. Bigot, *Phys. Rev. Lett.* **89**, 017401 (2002).
- [17] B. Koopmans, G. Malinowski, F. Dalla Longa, D. Steiauf, M. Fähnle, T. Roth, M. Cinchetti, and M. Aeschlimann, *Nat. Mater.* **9**, 259 (2010).
- [18] M. Battiato, K. Carva, and P. M. Oppeneer, *Phys. Rev. B* **86**, 024404 (2012).
- [19] I. A. Yastremsky, P. M. Oppeneer, and B. A. Ivanov, *Phys. Rev. B* **90**, 024409 (2014).
- [20] A. J. Schellekens, W. Verhoeven, T. N. Vader, and B. Koopmans, *Appl. Phys. Lett.* **102**, 252408 (2013).
- [21] E. Turgut *et al.*, *Phys. Rev. Lett.* **110**, 197201 (2013).

- [22] M. Lisowski, P. A. Loukakos, U. Bovensiepen, J. Stähler, C. Gahl, and M. Wolf, *Appl. Phys. A* **78**, 165 (2004).
- [23] M. Bonn, D. N. Denzler, S. Funk, M. Wolf, S.-S. Wellershoff, and J. Hohlfeld, *Phys. Rev. B* **61**, 1101 (2000).
- [24] E. D. Palik, *Handbook of Optical Constants*, Vols. 1 and 2 (Elsevier Science, 1998).
- [25] D. L. Windt, *Comput. Phys.* **12**, 360 (1998).
- [26] H.-S. Rhie, H. A. Dürr, and W. Eberhardt, *Phys. Rev. Lett.* **90**, 247201 (2003).
- [27] J. Hohlfeld, Ph.D. thesis, Freie Universität Berlin, 1998.
- [28] A. Tari, *The Specific Heat of Matter at Low Temperatures* (Imperial College Press, London, 2003).
- [29] C. Y. Ho, R. W. Powell, and P. E. Liley, *J. Phys. Chem. Ref. Data* **3**, Suppl. 1 (1974).
- [30] L. Yaws, *The Yaws Handbook of Physical Properties for Hydrocarbons and Chemicals* (Gulf Publishing Company, 2005).
- [31] M. E. Wieser and T. B. Coplen, *Pure Appl. Chem.* **83**, 359 (2010).
- [32] M. B. Stearns, in *3d, 4d, and 5d Elements, Alloys, and Compounds*, edited by H. P. J. Wijn, Vol. III/19a, Landolt Börnstein New Series (Springer, Berlin, 1986x).
- [33] J. Crank, *The Mathematics of Diffusion* (Oxford University Press, Oxford, 1980).
- [34] L. Braicovich and G. van der Laan, *Phys. Rev. B* **78**, 174421 (2008).
- [35] J. Hohlfeld, S.-S. Wellershoff, J. Güdde, U. Conrad, V. Jähnke, and E. Matthias, *Chem. Phys.* **251**, 237 (2000).
- [36] M. Sultan, A. Melnikov, and U. Bovensiepen, *Phys. Status Solidi B* **248**, 2323 (2011).
- [37] M. Sultan, U. Atxitia, A. Melnikov, O. Chubykalo-Fesenko, and U. Bovensiepen, *Phys. Rev. B* **85**, 184407 (2012).
- [38] L. Gonzalez, R. Miranda, M. Salmeron, J. A. Vergés, and F. Ynduráin, *Phys. Rev. B* **24**, 3245 (1992).
- [39] G. Traeger, L. Wenzel, and A. Hubert, *Phys. Status Solidi A* **131**, 201 (1992).
- [40] J. Zak, E. R. Moog, C. Liu, and S. D. Bader, *Phys. Rev. B* **43**, 6423 (1991).
- [41] I. Radu, G. Woltersdorf, M. Kiessling, A. Melnikov, U. Bovensiepen, J.-U. Thiele, and C. H. Back, *Phys. Rev. Lett.* **102**, 117201 (2009).
- [42] M. Battiato, Ph.D. thesis, Uppsala University, 2013.
- [43] For the transient response we multiply this with a Gaussian function with FWHM 35 fs according to the laser pulse duration of our experiment.
- [44] J. P. Perdew, K. Burke, and M. Ernzerhof, *Phys. Rev. Lett.* **77**, 3865 (1996).
- [45] G. Kresse and J. Hafner, *J. Phys.: Condens. Matter* **6**, 8245 (1994).
- [46] P. E. Blöchl, *Phys. Rev. B* **50**, 17953 (1994).
- [47] G. Kresse and D. Joubert, *Phys. Rev. B* **59**, 1758 (1999).
- [48] F. Vincent and M. Figlarz, C. R. Hebd. Seances Acad. Sci. C **264**, 1270 (1967).